Development of a CRISPR activation system for targeted gene upregulation in *Synechocystis* sp. PCC 6803

Barbara Bourgade[a,b], Hao Xie[a], Peter Lindblad[a] and Karin Stensjö[a,*]

[a]Microbial Chemistry, Department of Chemistry-Ångström Laboratory,

Uppsala University, Uppsala, Sweden

[b]Current address: Department of Organismal Biology, Uppsala University, Uppsala, Sweden

* Corresponding author: karin.stensjo@kemi.uu.se

Abstract

The photosynthetic cyanobacterium *Synechocystis* sp. PCC 6803 offers a promising sustainable solution for simultaneous CO_2 fixation and compound bioproduction. While various heterologous products have now been synthesised in *Synechocystis*, limited genetic tools hinder further strain engineering for efficient production. Here, we present a versatile CRISPR activation (CRISPRa) system for *Synechocystis*, enabling robust multiplexed activation of both heterologous and endogenous targets. Following tool characterisation, we applied CRISPRa to explore targets influencing biofuel production, specifically isobutanol (IB) and 3-methyl-1-butanol (3M1B), demonstrating a proof-of-concept approach to identify key reactions constraining compound biosynthesis. Notably, individual upregulation of target genes, such as *pyk1*, resulted in up to 4-fold increase in IB/3M1B formation while synergetic effects from multiplexed targeting further enhanced compound production, highlighting the value of this tool for rapid metabolic mapping. Interestingly, activation efficacy did not consistently predict increases in compound formation, suggesting complex regulatory interactions influencing bioproduction. This work establishes the first CRISPRa system in cyanobacteria, providing an adaptable platform for high-throughput screening, metabolic pathway optimisation and functional genomics. Our CRISPRa system provides a crucial advance in the genetic toolbox available for *Synechocystis* and will facilitate innovative applications in both fundamental research and metabolic engineering in cyanobacteria.

Introduction

Biological processes are increasingly recognised as robust sustainable alternatives to conventional chemical methods for the production of fuels and chemicals. Amongst these, photosynthetic cyanobacteria offer a promising strategy for simultaneous CO_2 fixation and compound bioproduction from sunlight, a critical approach to mitigate the escalating climate crisis. The model freshwater cyanobacterium *Synechocystis* sp. PCC 6803 (hereafter referred to as *Synechocystis*) has become a leading candidate in photosynthetic biotechnology, due to its well-characterised physiology and metabolism. Through the introduction of heterologous pathways and redirection of metabolic fluxes, *Synechocystis* has demonstrated its potential as a versatile microbial cell factory, enabling the laboratory-scale production of a wide range of compounds[1–7]. However, despite these advancements, engineering cyanobacteria as efficient microbial cell factories remains a significant challenge. In particular, the limited genetic toolkit in *Synechocystis*, substantially less developed than in model bacteria, restricts complex metabolic engineering, limiting efforts to optimise compound production.

In recent years, CRISPR-Cas (Clustered Regularly Interspaced Short Palindromic Repeats – CRISPR associated proteins) technologies have significantly expanded and accelerated the scope of genetic engineering[8], enabling precise gene-editing and transcriptional control. Particularly noteworthy are CRISPR interference (CRISPRi)[9] and CRISPR activation (CRISPRa)[10,11], which utilise catalytically deactivated Cas (dCas) enzymes to precisely regulate transcription. CRISPRi represses transcription by blocking transcription initiation or elongation while CRISPRa enhances transcription by recruiting RNA polymerase at a target locus. In prokaryotic systems, CRISPRa-mediated gene activation has been achieved using various mediators, such as the *Escherichia coli* transcriptional activator SoxS or RNA polymerase subunits[11,12], facilitated through synthetic protein fusions[13] or RNA-binding proteins, such as the bacteriophage MS2-MCP (MS2 coat protein) system[11,14]. These transient and reversible techniques allow systematic exploration of gene function and regulation as well as comprehensive metabolic studies to identify key reactions that limit compound biosynthesis. For example, CRISPRi libraries have been employed for genome-wide screens to assess gene essentiality under diverse growth conditions in *Synechocystis*, revealing essential metabolic processes required for survival in specific environments[15,16]. Targeted CRISPRi approaches have also been utilised to study photosynthetic complexes[17] and identify metabolic pathways constraining biosynthesis of target compounds[18]. Collectively, these studies highlight the broad applicability and significance of CRISPR-mediated regulatory tools. However, in contrast to CRISPRi, CRISPRa has yet to be established in cyanobacteria, despite its clear potential to facilitate rapid metabolic mapping and target discovery in both fundamental and applied research.

In this study, we report the development of a rhamnose-inducible CRISPRa system for targeted gene upregulation in *Synechocystis* using a dCas12-SoxS protein fusion (Fig. 1) to recruit RNA polymerase at specific promoters. Our system demonstrates reliable gene activation across various targets, with activation efficacy dependent on guide RNA (gRNA) position relative to the transcriptional start site (TSS) and the intrinsic strength of the target promoter. To further evaluate its applicability for metabolic engineering, we applied CRISPRa to upregulate key genes involved in the biosynthesis of the biofuel candidates isobutanol (IB) and 3-methyl-1-butanol (3M1B). This approach successfully identified specific genes that resulted in increased IB and 3M1B titres when upregulated, establishing a proof-of-concept application of CRISPRa for metabolic engineering in cyanobacteria, and further highlighted the complex and dynamic system-wide metabolic regulation influencing compound bioproduction. Our findings report the first cyanobacterial CRISPRa system, significantly expanding the genetic toolkit available for *Synechocystis*, and establish CRISPRa as a versatile and scalable platform to enhance cyanobacterial biotechnology, offering a powerful approach for optimising photosynthetic production of high-value compounds.

Results

Development and characterisation of a CRISPRa system for targeted gene upregulation in *Synechocystis*

To establish a CRISPRa system in *Synechocystis*, we fused the R93A variant[19] of the *E. coli* transcriptional activator SoxS to the C-terminus of *Francisella novicida* dCas12a mutant, previously used for CRISPRi in *Synechocystis* [17,18], with a 10-aa linker peptide[13] (Fig. 1). This fusion was expressed under the control of the rhamnose-inducible P_{rha} promoter[20], allowing precise induction of gene activation.

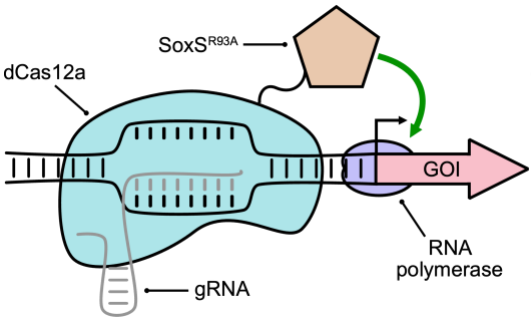

Figure 1. The developed CRISPRa system consisting of a protein fusion between *F. novicida* dCas12a and SoxS^{R93A}. Through gRNA-guided dCas12 binding at a specific site upstream the target promoter, RNA polymerase is recruited by SoxS to initiate transcription at the candidate promoter. GOI: gene of interest.

Prior studies of prokaryotic dCas9-based CRISPRa systems have demonstrated that the activation efficacy is highly sensitive to the position of the gRNA target site relative to the TSS of the candidate gene[19,21–24]. To assess whether this positional effect influences our dCas12-based CRISPRa system, we explored activation of a chromosomally integrated green fluorescent protein (GFP) gene driven by the strong constitutive P_{trc} promoter[25] using different gRNAs positioned across a 328-bp region upstream P_{trc} (Fig. 2). Our results showed clear GFP upregulation with gRNAs targeting sites between -97 and -328, indicating a flexible targeting range. Notably, gRNAs positioned between -97 and -156 produced the highest fluorescence levels, suggesting that this region represents the optimal targeting window for gene activation with dCas12-SoxS in *Synechocystis*, by effectively recruiting RNA polymerase to the target promoter. In contrast, a gRNA positioned at -48 showed no GFP activation, possibly due to disrupted interactions between SoxS and RNA polymerase. Additionally, previous studies have reported strand-specific differences in activation levels when targeting the DNA template strand versus non-template strand[23]. We further explored this behaviour using two overlapping pairs of gRNAs (-97 NTS/-108 and -144 NTS/-156) targeting the template or non-template strand within the optimal target window. Our results indicated that targeting the non-template strand led to enhanced fold-activation, providing an additional strategy for fine-tuning activation levels. Consistent with previous reports on dCas12-based systems[26], co-expression of two gRNAs (-108/-156) demonstrated a combinatorial effect, resulting in fold-activation levels exceeding those of the respective single gRNAs. Additionally, the CRISPRa system was also applicable for transient gene repression by directing it to *gfp* coding sequence (CDS), effectively blocking transcription elongation, as previously described for similar systems[13]. This dual capability for upregulation and downregulation provides the opportunity for complex metabolic rewiring through simultaneous targeting of multiple genes.

To assess the stability of this CRISPRa system, we monitored GFP fluorescence over a 96-hour post-induction period using four selected gRNAs (-48; -108; -156 and CDS). GFP upregulation was maintained throughout this period (Supplementary Fig. 1), highlighting the system's applicability for target mapping over multiple days. Moreover, based on prior results showing effective CRISPRi repression with 3 mM of rhamnose[18], our initial characterisation was conducted with 3 mM of rhamnose. We subsequently explored whether higher inducer concentrations correlated with increased activation levels by testing the effect of 6 or 9 mM of rhamnose on GFP activation with selected gRNAs (-97 NTS; -108; -144 NTS and -156). These results indicated that increased rhamnose concentrations did not correspond to higher fold-activation (Supplementary Fig. 2), suggesting a saturation point for inducer efficacy. Based on this, we conducted subsequent experiments using 3 mM of rhamnose for CRISPRa induction.

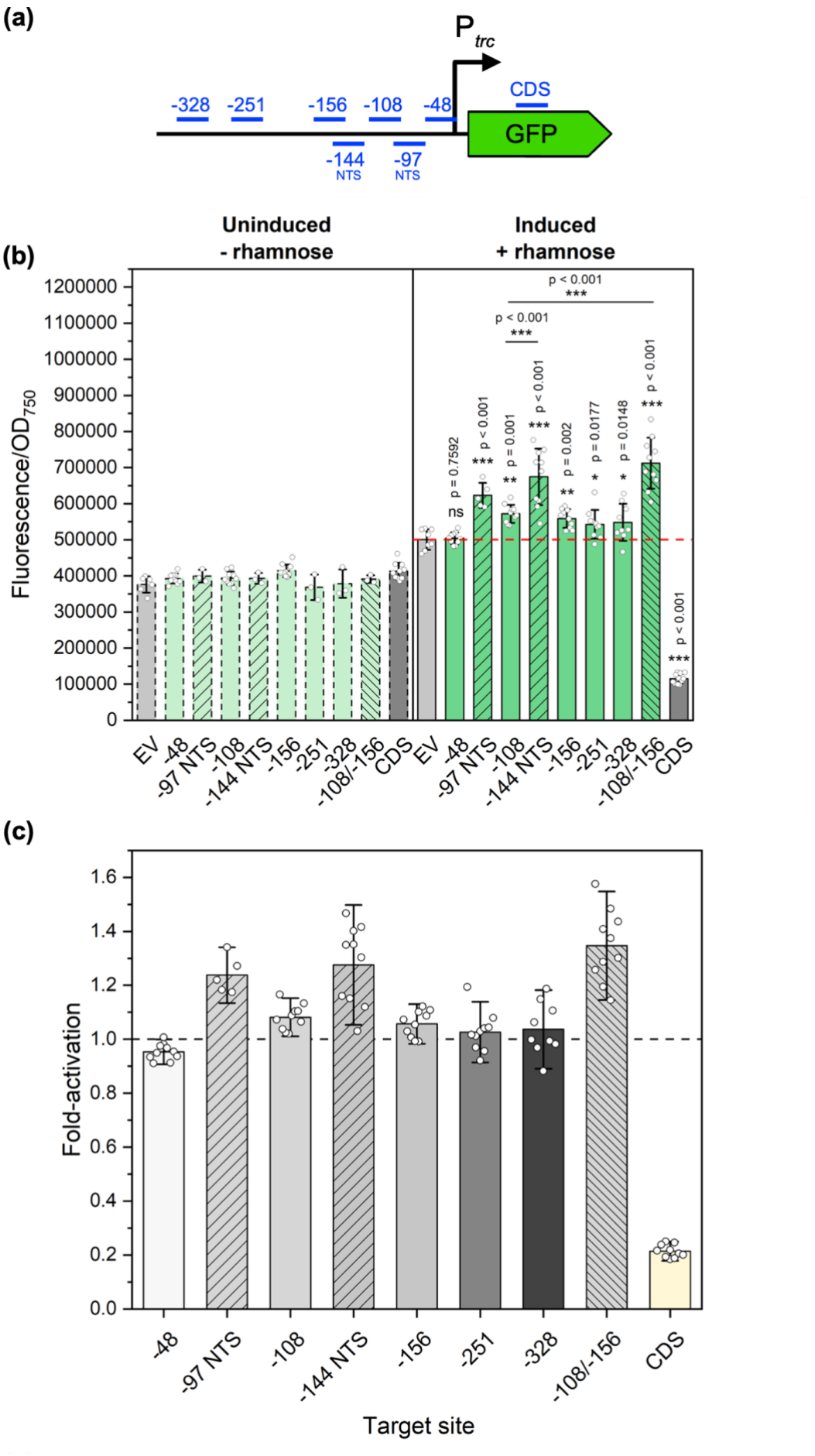
(a)
P trc
CDS
-328
-251
-156
-108
-48
GFP
-144 NTS
-97 NTS
(b)
Uninduced - rhamnose
Induced + rhamnose
Fluorescence/OD750
EV
-48
-97 NTS
-108
-144 NTS
-156
-251
-328
-108/-156
CDS
p = 0.7592
ns
p < 0.001
p = 0.001
p = 0.002
p = 0.0177
p = 0.0148
(c)
Fold-activation
Target site

Figure 2. **GFP fluorescence at 72 hours post-induction with 3 mM rhamnose with eight gRNAs targeting P_{trc} with dCas12-SoxS.** (a) Seven gRNAs were designed to target a 328-bp region upstream P_{trc} driving GFP expression, with an additional gRNA targeting the coding sequence. (b) GFP fluorescence was measured in the absence or presence of the rhamnose inducer across 8 candidate gRNAs. (c) Fold-activation of GFP was determined relative to the negative control (EV) for each candidate gRNA. GFP: green fluorescent protein; NTS: non-template strand; EV: negative control; CDS: coding sequence. Error bars indicate standard deviation (- rhamnose samples: EV: n=6; -48, -108, -156, CDS: n=10; -97 NTS, -144 NTS, -251, -328, -108/-156: n=3; + rhamnose samples: EV: n=8; -97 NTS: n=5; other gRNAs: n=10). p value representation: ns > 0.05; * < 0.05; ** < 0.01; *** < 0.001. p value was calculated by comparing each sample to the negative control unless otherwise stated.

Promoter strength-dependent activation levels using the CRISPRa dCas12-SoxS system

Previous prokaryotic CRISPRa systems have demonstrated that activation levels are closely linked to the intrinsic strength of the target promoter[19,23], with minimal response observed for strong promoters and high fold-activation achieved with weaker promoters. To investigate whether this effect occurs with our CRISPRa system, we selected four synthetic promoters from the modified BioBrick_J231XX series, previously characterised in *Synechocystis*[27]. These promoters differ by specific point mutations within the promoter sequence, allowing us to use the same gRNA to target upstream all promoters and thereby isolate the effects of promoter strength from those of gRNA positioning and sequence. Consistent with previous reports[19,23], our results indicated that activation was indeed stronger for weaker promoters (Fig. 3). Notably, we achieved a 2.28 (± 0.57) fold-activation with the weakest promoter tested, J23101, compared to 1.21 (± 0.10) with the strong promoter J23116. These findings suggest that basal promoter strength is a key factor in determining fold-activation in response to targeting with our CRISPRa system, which may constrain upregulation of endogenous genes.

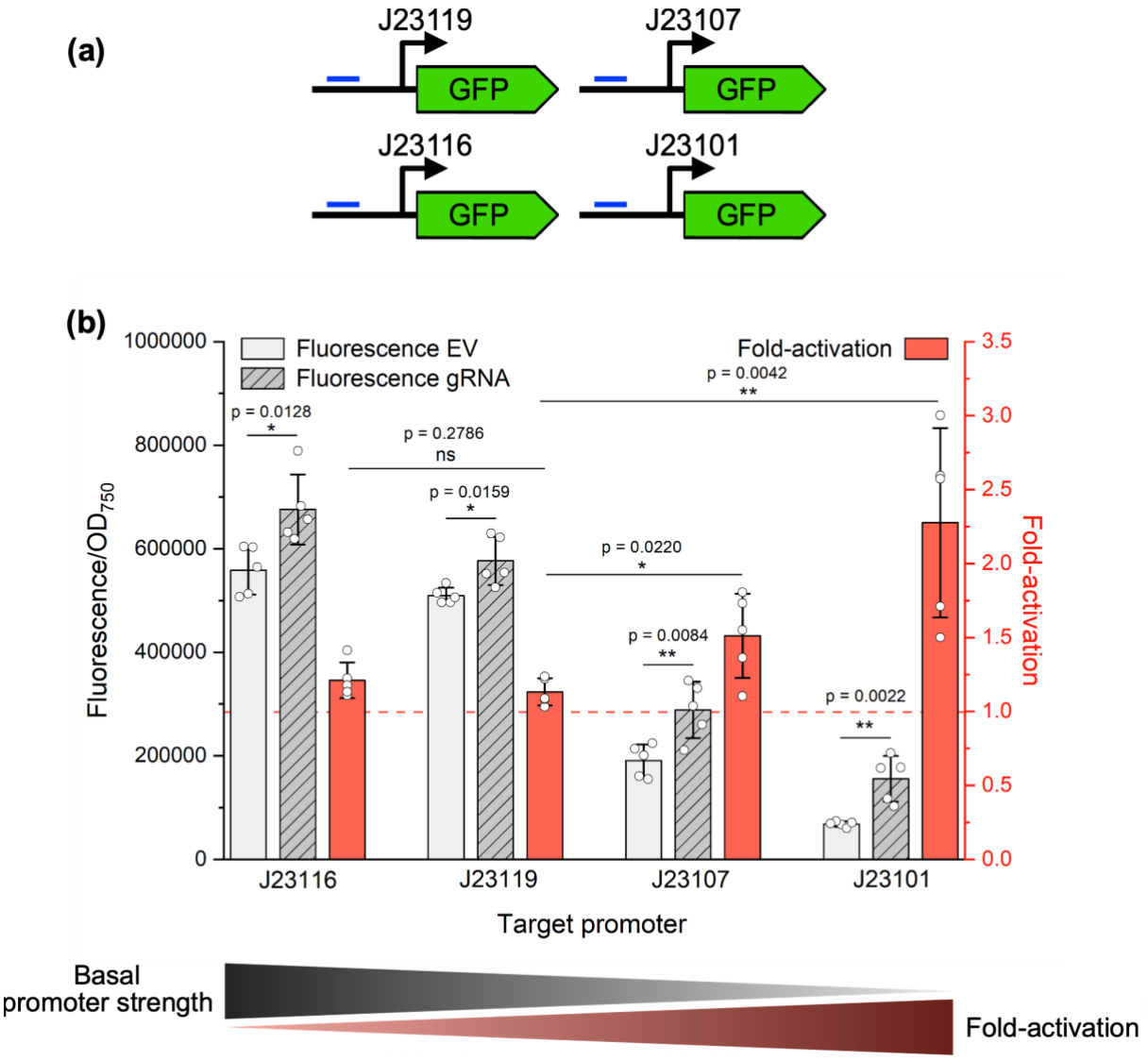

Figure 3. Correlation between promoter strength and activation levels with the dCas12-SoxS CRISPRa system. (a) Four synthetic promoters of the Biobrick J23 series were selected and tested for activation with dCas12-SoxS using a common gRNA. (b) Fluorescence (gray) and activation (red) levels were measured following rhamnose induction of the dCas12-SoxS system for the four J23 promoters. Error bars indicate standard deviation (n=5). p value representation: ns > 0.05; * < 0.05; ** < 0.01; *** < 0.001.

CRISPRa-mediated upregulation of *kivD*^{S286T} for enhanced isobutanol and 3-methyl-1-butanol biosynthesis in *Synechocystis*

To evaluate the applicability of our CRISPRa system for metabolic engineering in *Synechocystis*, we investigated CRISPRa-mediated upregulation of the engineered *kivD*^{S286T} gene[28], which encodes an α-ketoisovalerate decarboxylase, enabling the biosynthesis of isobutanol (IB) and 3-methyl-1-butanol (3M1B) from 2-ketoisovalerate and 2-ketoisocaproate, respectively, in *Synechocystis*. Our experiments included three background strains: ddh_kivD

(obtained with plasmid pHX8[29]; single *kivD*^{S286T} copy inserted at the *ddh* site), HX11 (as detailed in Xie et al., 2024[18]; two *kivD*^{S286T} copies inserted at the *ddh* and NS1[4] *(slr0168)* sites) and HX51 (Xie and Lindblad, unpublished; three *kivD*^{S286T} copies inserted at the *ddh*, NS1 and *sll1564*[4] sites). These strains contained one, two or three chromosomally-integrated copies of *kivD*^{S286T} under the control of the P_{trc} promoter (Fig. 4) and were subjected to single, dual and triple CRISPRa targeting.

IB and 3M1B production was monitored over 10 days, with day 4 consistently showing the highest CRISPRa-induced improvement across all strains (Fig. 4; Supplementary Fig. 3). At later timepoints, IB and 3M1B levels became comparable between CRISPRa-targeted and non-targeted strains. Notably, only modest improvements in product titres were achieved with CRISPRa-mediated *kivD*^{S286T} upregulation across most gRNA combinations. In HX51-derived strains, only dual and triple targeting showed slight improvements in IB and 3M1B production, suggesting that single targeting was insufficient to enhance product titres in this background strain. These findings indicate that elevated expression of the key biosynthetic gene may not directly translate to higher product titres, potentially due to substrate limitations acting as a bottleneck for product formation.

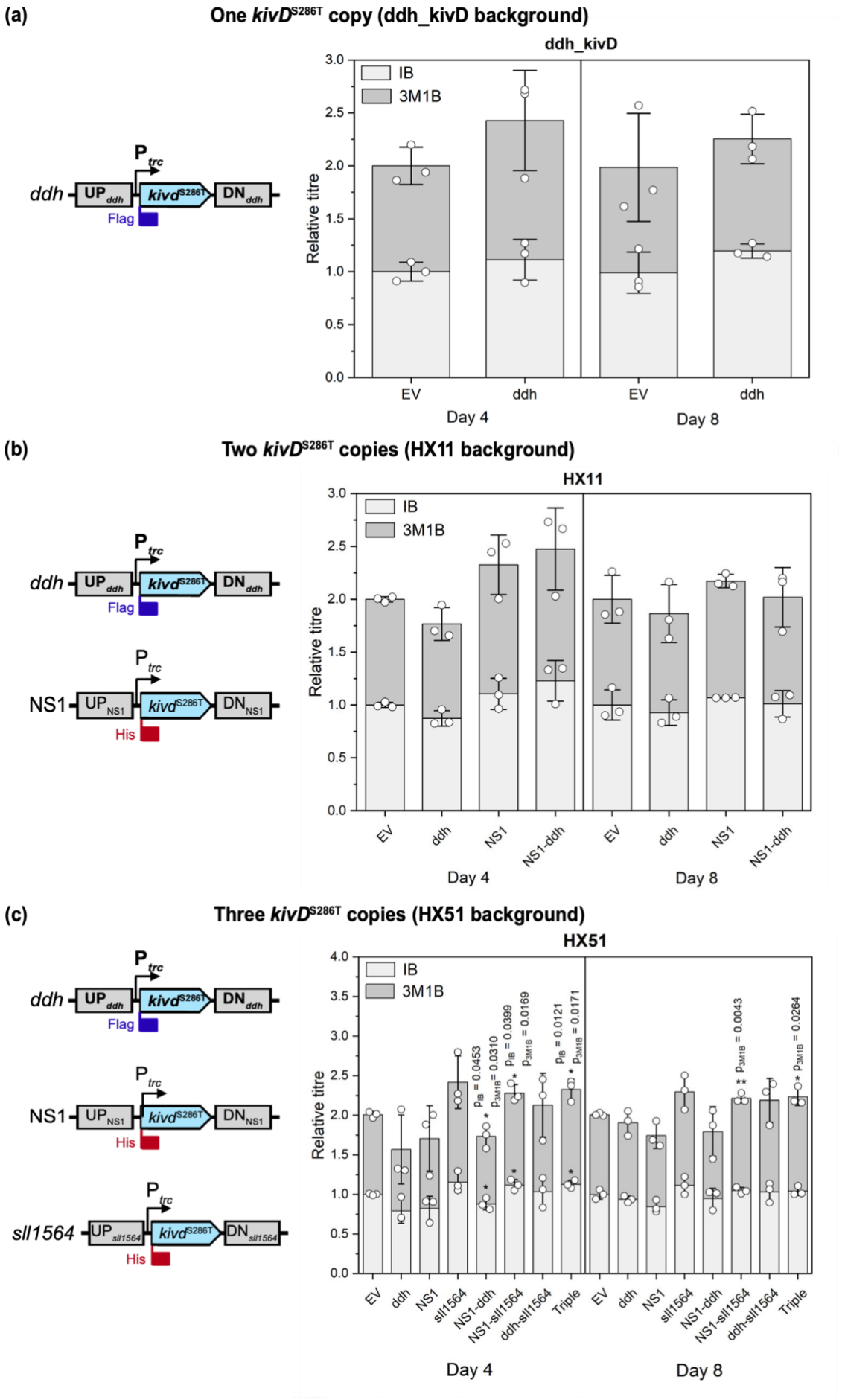
(a)
One kivD S286T copy (ddh_kivD background)
ddh_kivD
IB
3M1B
Relative titre
EV
ddh
Day 4
Day 8
(b)
Two kivD S286T copies (HX11 background)
HX11
NS1
NS1-ddh
(c)
Three kivD S286T copies (HX51 background)
HX51
sll1564
ddh-sll1564
Triple
Flag
His

Figure 4. Relative isobutanol (IB) and 3-methyl-1-butanol (3M1B) titres on days 4 and 8 in response to CRISPRa-mediated *kivD*^{S286T} upregulation. Single, dual, and triple CRISPRa targeting using different gRNA combinations were assessed in three background strains: (a) ddh_kivD (harboring one copy of *kivD*^{S286T}), (b) HX11 (two copies of *kivD*^{S286T}), and (c) HX51 (three copies of *kivD*^{S286T}), as shown in the corresponding construct schematics. EV: negative control; UP: upstream homology arm; DN: downstream homology arm. Error bars indicate standard deviation (n=3). p value representation: * < 0.05; ** < 0.01.

Additionally, gRNA performance varied depending on the strain background. For instance, dual targeting of the NS1 and *ddh* loci resulted in opposite effects on IB and 3M1B production in HX11 and HX51, despite the identical *kivD*^{S286T} constructs and gRNAs used for gene activation, indicating that genetic context of the respective strains rather than gRNA efficiency may account for these differences. Unexpectedly, CRISPRa targeting led to a modest reduction in IB and 3M1B production in several strains, particularly prevalent in HX51 derivatives. Analysis of relative *kivD*^{S286T} transcript levels on day 4 (Fig. 5) confirmed that CRISPRa-mediated upregulation was effective in some strains, although this did not consistently correlate with proportional improvements in product titres. For example, despite a 3.19 (± 0.24) fold-activation in the targeted ddh_kivD strain, only marginal improvements in IB and 3M1B formation were observed. In HX11-derived strains, lower activation levels and delayed growth (Supplementary Fig. 3) suggest that the reduced response may be linked to an unidentified phenotype in the HX11 background strain. In HX51 derivatives, fold-activation generally correlated with product titres, confirming that single targeting unexpectedly led to *kivD*^{S286T} downregulation. However, transcript levels of *kivD*^{S286T} at the NS1 and *sll1564* sites could not be differentiated in qPCR readings, limiting our ability to fully characterise the tool's behaviour in these strains. Collectively, these findings highlight the complexity of CRISPRa-mediated metabolic engineering in *Synechocystis*, suggesting that factors beyond transcriptional upregulation, such as substrate availability and strain-specific genetic context, play critical roles in determining biosynthetic output.

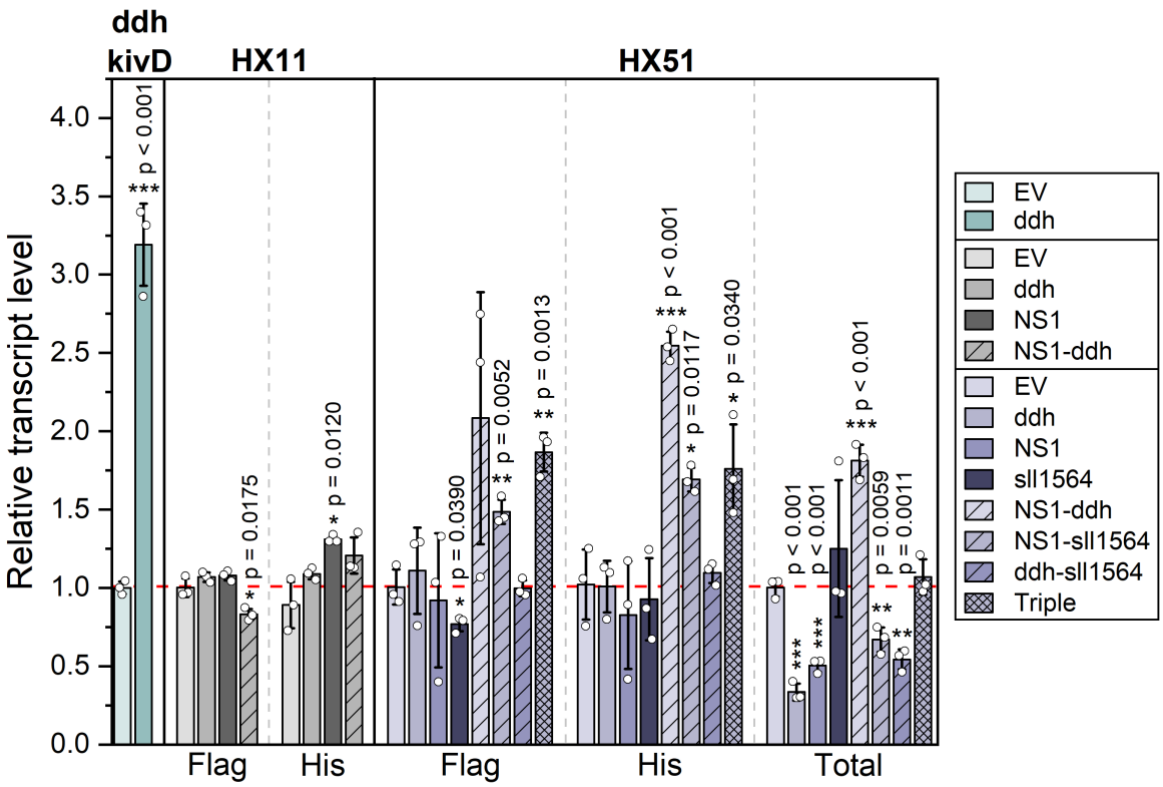

Figure 5. Relative *kivD*^{S286T} transcript levels at day 4 in CRISPR-activated strains. Gene expression was quantified with different primer sets designed to bind within the coding sequence (Total), the Flag tag (Flag) or the His tag (His) to differentiate which *kivD*^{S286T} was activated when applicable. EV: negative control. Error bars indicate standard deviation (n=3). p value representation: * < 0.05; ** < 0.01; *** < 0.001.

CRISPRa-mediated metabolic mapping to identify candidate genes enhancing IB and 3M1B biosynthesis

To investigate CRISPRa-mediated target mapping for optimising metabolic engineering strategies, we applied our system to upregulate candidate genes (Fig. 6) hypothesised to influence pyruvate formation and cofactor availability, both potentially limiting IB/3M1B biosynthesis. We upregulated *pyk1* (*sll0587*) and *pyk2* (*sll1275*)[30], encoding pyruvate kinase 1 and 2, respectively, to increase the conversion of phosphoenolpyruvate (PEP) to pyruvate. Additionally, we explored enhancing pyruvate availability by targeting *me* encoding a malic enzyme[31], which catalyses the oxidation of malate to pyruvate, as previous studies have demonstrated that *me* overexpression leads to increased formation of pyruvate-derived products, such as lactate[32]. To further channel carbon flow from CO_2 fixation towards pyruvate formation, we targeted triosephosphate isomerase (TPI), which converts dihydroxyacetone phosphate (DHAP) into glyceraldehyde-3-phosphate (G3P) in the Calvin-Benson-Bassham (CBB) cycle. This approach has previously increased phloroglucinol biosynthesis in *E. coli*[33]

while overexpression of *E. coli* TPI, in conjunction with other enzymes, has improved IB/3M1B formation[4] in *Synechocystis*. In addition to genes involved in pyruvate formation, we also targeted two additional genes relevant for cofactor availability, specifically NADPH, hypothesising that limited availability of NADPH may constrain the conversion of 2-acetolactate to 2,3-dihydroxyisovalerate[34], as reported in other organisms[35], as well as the conversion of isobutylaldehyde and 3-methylbutyraldehyde into the respective products IB and 3M1B. In a previous study, overexpression of *pntAB*, coding for a membrane-bound pyridine nucleotide transhydrogenase, slightly increased L-valine biosynthesis in *E. coli*, by promoting cofactor regeneration[35]. We thus chose to target *pntA* for upregulation, although it has previously been reported that PntA is particularly important for cofactor regeneration under mixotrophic growth conditions but is dispensable under phototrophic conditions[36] in *Synechocystis*. Lastly, we targeted *petH*, encoding a ferredoxin-$NADP^+$ oxidoreductase (FNR), a key enzyme for NADPH regeneration in the photosynthetic electron transport chain[37], which has been demonstrated to increase intracellular NADPH levels when overexpressed in *Synechocystis*[38]. For three selected genes (*pyk1*, *pyk2* and *pntA*), we tested two different gRNAs, referred to as gene.1 and gene.2 on Fig. 7 and Supplementary Fig. 6, both targeting within the optimal targeting window between -100 to -150 bp upstream the TSS, in order to investigate the impact of the gRNA sequence on activation levels.

Upon CRISPRa targeting, IB and 3M1B biosynthesis was increased for most targets (Fig. 7), although some targets displayed only transient effects. In particular, upregulation of genes hypothesised to affect pyruvate availability, as exemplified by gRNAs pyk2.2 and tpi, improved IB/3M1B primarily at early growth stages, with minimal effects on day 4 (Fig. 7a, b). In contrast, activation of *petH* sustained increased product biosynthesis throughout the experimental period. Notably, across all targets, improvements were more pronounced for 3M1B than IB, reaching up to ~3.5-fold improvement on day 2 (Fig. 7c). Additionally, negligible differences in compound production were detected between the two candidate gRNAs for *pyk1, pyk2* and *pntA*, suggesting minimal influence of gRNA sequence within the optimal targeting window. However, strains targeting *pyk1* and *pyk2* displayed distinct production profiles, highlighting their unique roles and regulation. Notably, strains with *pyk1* activation exhibited high biological variability, associated with impaired growth (Supplementary Fig. 4), particularly noticeable with gRNA pyk1.2. These strains also displayed a significant shift of IB/3M1B ratio (Fig. 7d), indicating substantial metabolic disruption. Although the IB/3M1B ratio was also affected across several targets on day 2 (Supplementary Fig. 5), *pyk1* activation led to the most pronounced and lasting effect throughout the experiment, which requires further system-wide exploration to elucidate.

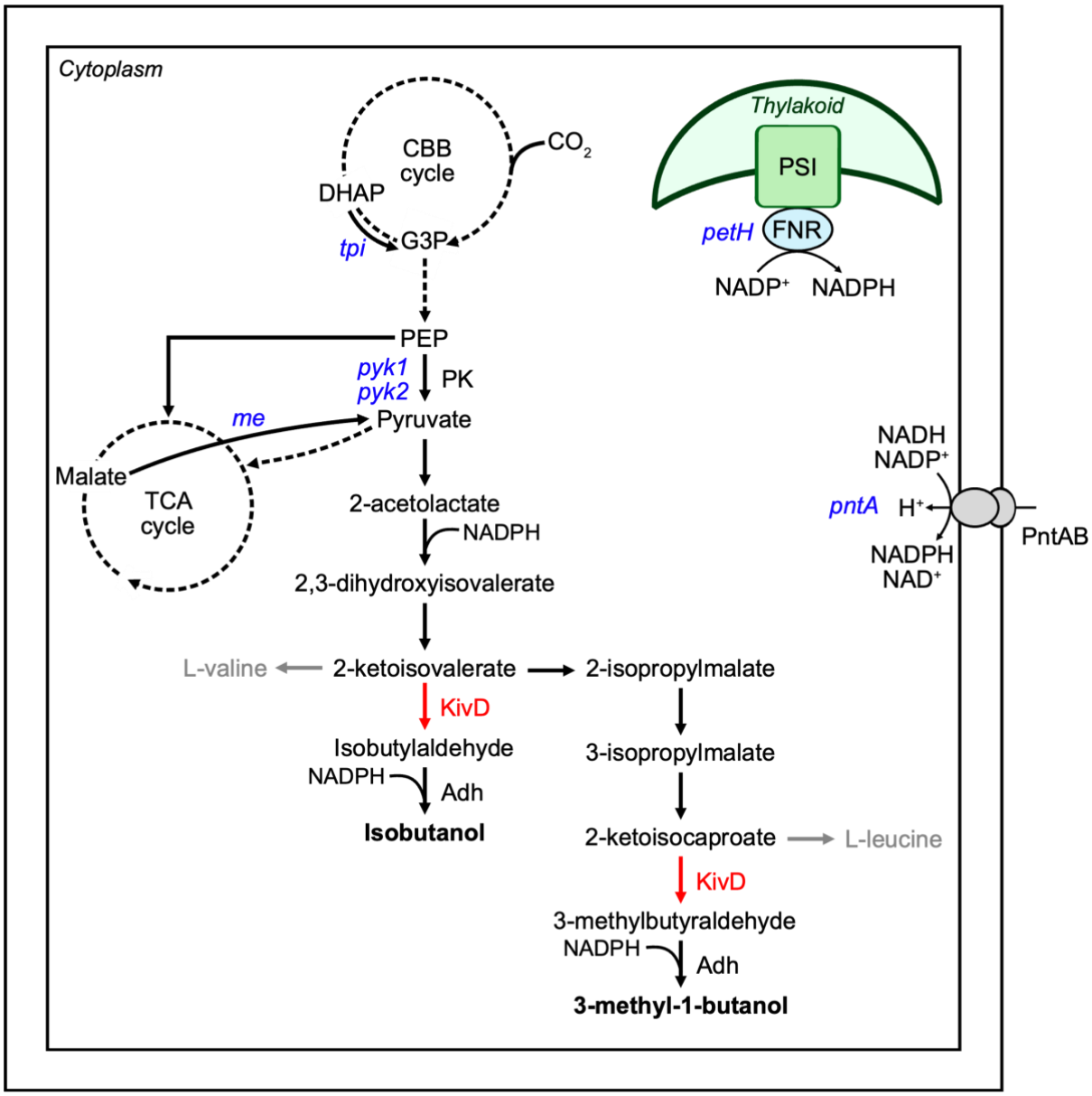

Figure 6. Simplified biosynthetic pathway for isobutanol and 3-methyl-1-butanol formation in *Synechocystis*. The key heterologous enzyme KivD (red) catalyses the conversion of 2-ketoisovalerate and 2-ketoisocaproate into isobutylaldehyde and 3-methylbutyraldehyde, respectively, which are subsequently converted into isobutanol and 3-methyl-1-butanol by *Synechocystis* alcohol dehydrogenase (Adh). Genes (blue) targeted by the CRISPRa system were selected to enhance pyruvate formation and NADPH regeneration, hypothesised as key bottlenecks for IB/3M1B biosynthesis. Abbreviations: Adh: alcohol dehydrogenase; CBB cycle: Calvin-Benson-Bassham cycle; DHAP: dihydroxyacetone phosphate; FNR: ferredoxin-$NADP^+$ oxidoreductase; G3P: glyceraldehyde-3-phosphate; KivD: α-ketoisovalerate decarboxylase; ME: malic enzyme; PEP: phosphoenolpyruvate; PK: pyruvate kinase; PntAB: pyridine nucleotide transhydrogenase; PSI: photosystem I; TCA cycle: tricarboxylic acid cycle.

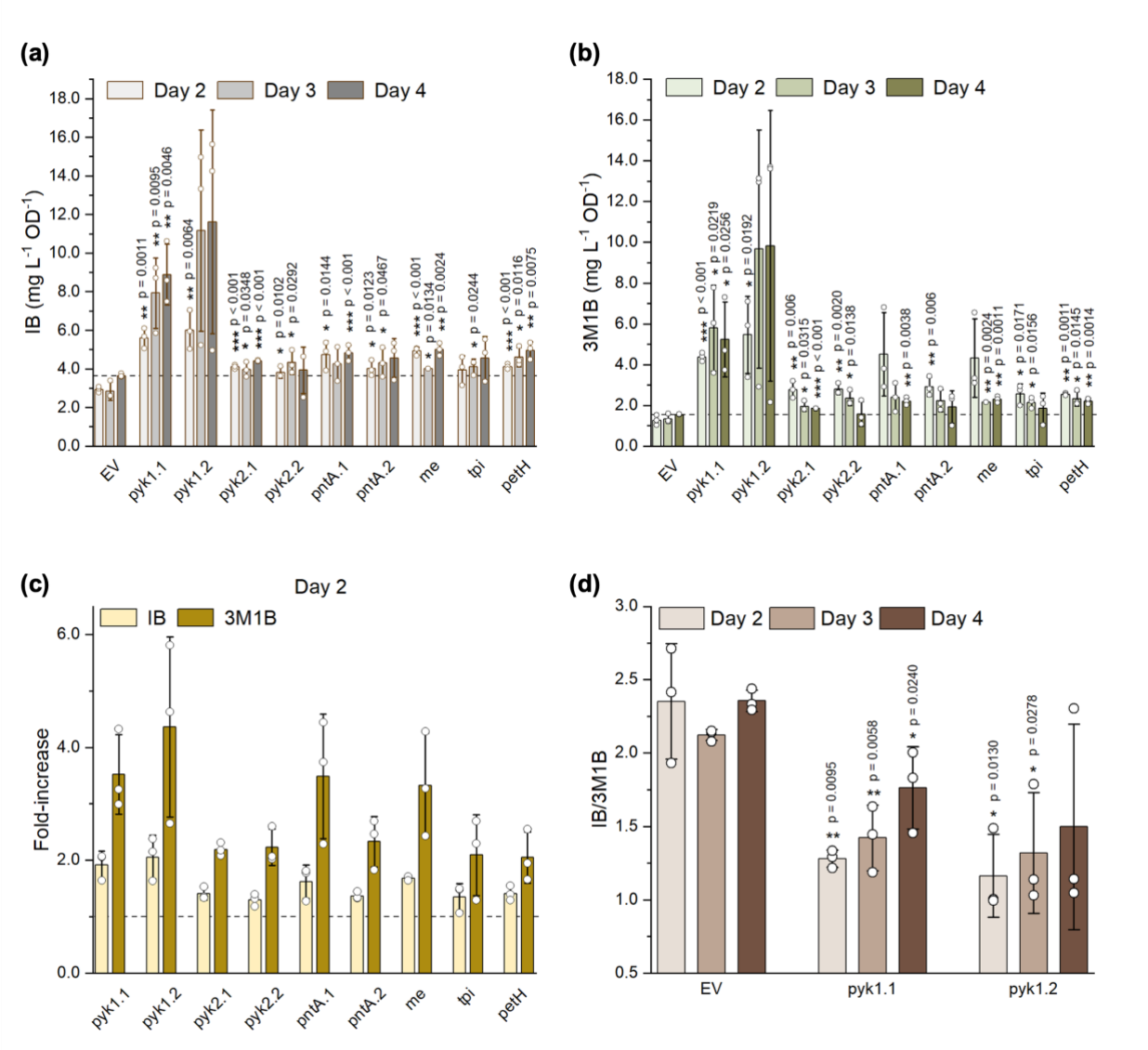

Figure 7. Isobutanol and 3-methyl-1-butanol production in response to CRISPRa targeting of select genes involved in pyruvate formation and NADPH regeneration. (a) Isobutanol titres on days 2, 3 and 4. (b) 3-methyl-1-butanol titres on days 2, 3 and 4. (c) Fold-increase of isobutanol and 3-methyl-1-butanol relative to the negative control (EV) on day 2. (d) IB/3M1B ratio for *pyk1* activation. gene.1 and gene.2 refers to gRNAs #1 and #2, respectively, when applicable. EV: negative control; IB: isobutanol; 3M1B: 3-methyl-1-butanol. Error bars indicate standard deviation (n=3). p value representation: * < 0.05; ** < 0.01; *** < 0.001.

We confirmed successful upregulation of all candidate genes upon CRISPRa targeting, with strong activation observed across most targets (Supplementary Fig. 6). Minimal variation was detected between different gRNAs targeting the same gene, highlighting the efficacy of targeting within the optimal window to achieve robust activation, even for endogenous genes. However, this pattern did not extend to *pyk2*, suggesting that further gRNA optimisation may

be necessary for specific targets. Importantly, we found no direct correlation between activation efficiency and production increase, as demonstrated by the moderate improvements in product formation when activating *petH*, despite its strong activation. These results highlight that system-wide regulatory and metabolic factors may limit production outcomes, despite efficient gene upregulation.

Combinatorial effects of CRISPRa/i multiplexing on IB/3M1B biosynthesis

To further validate our earlier findings on the multiplexing capability of our CRISPRa system, we extended this approach in the context of metabolic engineering. Specifically, we targeted single genes with multiple gRNAs and simultaneously activated multiple genes for a subset of our candidate genes described in the previous section. Additionally, we aimed to downregulate two genes, namely *acnSP* and *slr6040* (Supplementary Fig. 7), with our novel CRISPRa system. The *acnSP* gene[39] encodes a 44-amino acid small protein previously shown to regulate the activity of the aconitase AcnB, which catalyses the conversion of citrate to isocitrate in the TCA cycle. Deletion of *acnSP* has been reported to cause significant metabolic perturbations, notably increasing levels of pyruvate-derived metabolites, including the branched-chain amino acids L-valine and L-leucine. *slr6040*[40,41] encodes a putative two-component response regulator, potentially involved in osmotic response. Shi et al.[41] demonstrated that a Δ*slr6040* mutant exhibited pronounced metabolic shifts, particularly in the TCA cycle, and a ~5-fold increase in pyruvate levels, particularly relevant for IB/3M1B biosynthesis. In addition to downregulating *acnSP* and *slr6040* individually, we also explored combining this downregulation with the upregulation of selected genes, further demonstrating the versatility of our CRISPRa system for metabolic mapping and production optimisation.

Based on our previous findings that the strongest impact on product formation was detected at day 2, we measured IB and 3M1B biosynthesis on day 2 for a combination of candidate genes (Fig. 8), all involved in pyruvate metabolism. In contrast to our results on fluorescence-based tool characterisation, targeting either *pyk1* or *pyk2* with two gRNAs did not further enhance product formation compared to single gRNAs (Fig. 8a). However, simultaneous activation of two genes showed combinatorial effects (Fig. 8b), achieving up to a 6-fold improvement in 3M1B production compared to single targets (Fig. 8d). Furthermore, single downregulation of *slr6040* and *acnSP* did not significantly improve product formation under the tested conditions (Fig. 8c). Interestingly, despite these marginal improvements for single downregulation, a notable combinatorial effect was observed when combining *acnSP* downregulation with *me* activation (Fig. 8c; 8d), reaching 3-fold increase in IB and 3M1B production compared to single targeting. However, multiplexing *slr6040* repression with *me* activation did not lead to combinatorial effects. Surprisingly, co-targeting *slr6040* and *me*

negatively impacted product formation, particularly IB biosynthesis, suggesting an unknown metabolic or regulatory interaction in this strain.

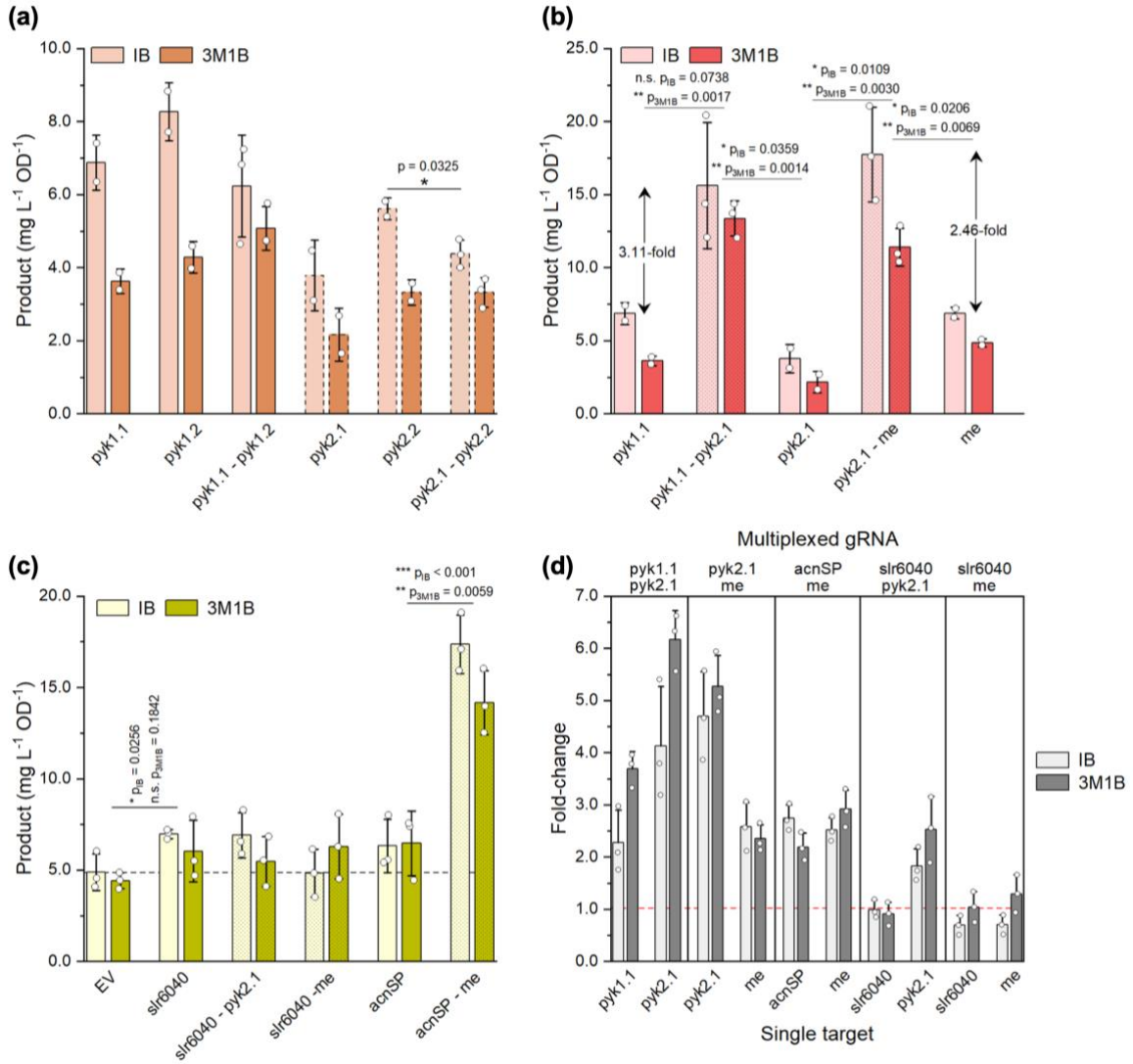

Figure 8. IB/3M1B biosynthesis in response to CRISPRa multiplexing for simultaneous down- and up-regulation of several target genes. (a) Targeting of *pyk1* or *pyk2* with two gRNAs. *pyk2* strains are represented with bars with a dashed outline. (b) Simultaneous activation of *pyk1* and *pyk2* or *pyk2* and ME. Fold-improvement are shown as the mean fold-change in IB and 3M1B production. (c) Downregulation of *slr6040* and *acnSP* using single or multiplexed gRNAs. (d) Fold-change of IB and 3M1B biosynthesis in multiplexed strains compared to single gRNA-targeted strains. EV: negative control; IB: isobutanol; 3M1B: 3-methyl-1-butanol. Error bars represent standard deviation (single activation: n=2; single repression and multiplexed targeting: n=3). p value representation: n.s. > 0.05; * < 0.05; ** < 0.01; *** < 0.001.

Although synergetic effects were not observed in all multiplexed strains, the CRISPRa system functioned as anticipated, achieving robust gene repression and activation across most

targets (Supplementary Fig. 8). Notably, no dilution effect was detected when simultaneously targeting multiple loci, demonstrating the system's capacity for effective multiplexed gene regulation. Unexpectedly, *me* transcript levels were reduced when co-targeting with *acnSP* repression, even though the identical *me*-specific gRNAs was used across all *me*-targeted strains. Additionally, in contrast to our previous findings, targeting *pyk1* or *pyk2* with dual gRNAs did not further enhance target activation, aligning with the product formation levels detected.

Discussion

In this study, we developed a dCas12a-mediated CRISPR activation system for targeted gene upregulation in *Synechocystis*, reporting the first CRISPRa tool established for cyanobacteria. Our initial characterisation experiments revealed that the designed tool exhibits a flexible editing window, with minimal differences between gRNAs targeting an optimal region approximately -100 to -200bp upstream of the TSS. In contrast to previously reported Cas9-based CRISPRa systems in other prokaryotes, which demonstrate significant changes in activation levels at a single-nucleotide resolution[12,19,23], our system offers greater flexibility, particularly advantageous for targeting endogenous promoters with limited PAM sequences. Furthermore, we observed increased activation at two separate loci when targeting the non-template strand opposite the promoter direction, providing an additional strategy to fine-tune activation levels for future applications. Consistent with previous studies in other prokaryotes[19,23] despite *Synechocystis* unique regulatory mechanisms, activation levels were found to be inversely correlated with the baseline expression levels of the target promoter, with weaker promoters showing a higher fold-increase than strong promoters. While this characterisation allows us to predict tool behaviour, other factors, such as the DNA sequence between the gRNA target site and the promoter[19,23], have been shown to influence activation levels but were not explored here. Future studies could thus investigate these parameters to refine CRISPRa efficiency in *Synechocystis* and reach maximal activation for synthetic genetic constructs. Notably, despite characterisation efforts, the fold-change in gene expression achieved in *Synechocystis* was significantly lower than in other organisms, where increases of ~50-to-100-fold[19,23] have been reported. This difference may be intrinsic to *Synechocystis* as an early transcriptomics analysis[42] under stress conditions suggested that its native transcriptional regulatory mechanisms exhibit a narrow dynamic range, further supported by studies focusing on specific stress conditions[43,44] or mutant strains[45].

We further investigated the potential of our CRISPRa system for metabolic engineering by activating the *kivD*^{S286T} gene[28] at the P_{trc} promoter to enhance isobutanol and 3-methyl-1-butanol production. Using both single or multiplexed gRNAs, we upregulated 1-to-3 copies of

kivD^{S286T} in three separate background strains. While transcript levels of *kivD*^{S286T} were successfully increased in most strains, this strategy only resulted in marginal improvements in IB and 3M1B biosynthesis. Although KivD has previously been identified as a critical bottleneck in this biosynthetic pathway[28,29], additional regulatory mechanisms, specifically those impacting intermediate availability, may be limiting IB and 3M1B formation. The native regulation of the branched-chain amino acid biosynthesis in *Synechocystis* remains largely unexplored but directly influences IB/3M1B formation. In other organisms, tight transcriptional and enzymatic control, with negative feedback loops and allosteric inhibition, respectively, has been shown to limit intermediate formation in this metabolic pathway[46], which may explain the modest improvements observed in our experiments. We, thus, suggest that future metabolic engineering efforts should focus on addressing these potential regulatory constraints to substantially enhance cyanobacterial IB/3M1B biosynthesis. Unexpectedly, we observed differing behaviour of identical gRNAs in separate background strains. While the precise cause of this variation remains unclear and requires additional work to elucidate, we hypothesise that this behaviour is not directly related to the CRISPRa system itself. Instead, this may be due to mutation or recombination events occurring in different background strains. Genetic instability has previously been recognised as a key challenge in cyanobacterial producer strains[47], although recent work in *Synechococcus elongatus* PCC 7942 demonstrated that targeted genetic engineering was required to increase mutation rates[48]. In addition to mutational events in genes involved in product formation, uncontrolled phenotypic instability[49], currently poorly understood, may also contribute to the differential behaviour observed, highlighting the need for a more comprehensive system-wide understanding of producer strain dynamics.

Furthermore, we targeted six native genes, associated with pyruvate formation and NADPH regeneration, with our CRISPRa system, facilitating rapid target mapping to identify metabolic processes relevant for IB and 3M1B biosynthesis. All candidates demonstrated robust activation, validating the CRISPRa system's applicability for precise upregulation of endogenous genes. However, activation levels did not directly correlate with fold-changes in product formation, indicating that a complex and dynamic regulation on a system-wide level influences compound production. While most targets led to increased product formation, upregulation of *pyk1* had the most pronounced effect on IB/3M1B levels, resulting in up to 4-fold increase on day 2. Notably, gene activation of some targets, such as *tpi* or *pntA*, only showed transient effects on compound bioproduction. We hypothesise that this phenomenon is due to native regulatory mechanisms governing these reactions, particularly important during early growth phases. These findings not only demonstrate the potential of the CRISPRa system for metabolic mapping but also provide insights into the metabolic processes influencing IB/3M1B biosynthesis in *Synechocystis*, which may extend to other compounds,

such as isobutene[7], originating from 2-ketoacid intermediates. Differential improvements observed between *pyk1* and *pyk2* activation suggest distinct regulatory mechanisms controlling these two targets, consistent with previous studies[30,50]. While transcriptional regulation of both *pyk1* and *pyk2* is responsive to glucose concentrations[51], Pyk1 is inhibited by high ATP levels[50], suggesting that it is inactive during photoautotrophic growth in response to high ATP levels generated during photosynthesis[31]. Conversely, Pyk2 regulation is linked to accumulation of sugar phosphates[30], hypothesised to be essential for sugar catabolism under hetero- or mixo-trophic conditions. Despite these reported regulatory mechanisms, the high activation levels achieved for both genes suggest that regulation governing these enzymes was less stringent in our experiments, allowing significant upregulation through CRISPRa targeting. Additionally, we observed enhanced IB/3M1B biosynthesis when upregulating *me*. Malate oxidation by ME has previously been reported as a key route for pyruvate formation[52], potentially bypassing pyruvate kinase, which potentially contributed to elevated pyruvate availability in our experiments, improving IB/3M1B biosynthesis. While a previous study showed that ME overexpression did not enhance ethanol production under photoautotrophic conditions[53], it did increase D-lactate biosynthesis under dark anoxic conditions[32]. Although ^{13}C flux analysis has previously reported that ME is active under light conditions[52], the role of light regulation in ME function remains unclear. Therefore, the improved IB/3M1B production observed in response to *me* upregulation could be attributed to both increased pyruvate formation and additional metabolic effects. As ME-dependent oxidation of malate derived from the TCA cycle has been shown to generate NADPH[31], we cannot exclude the possibility that *me* activation contributed to NADPH regeneration, important for IB/3M1B biosynthesis. *tpi* upregulation also led to modest improvements in IB/3M1B production, in accordance with previous results[5]. Collectively, our results further support that pyruvate availability represents a key bottleneck in IB/3M1B biosynthesis and requires additional engineering efforts for sustained improvement of IB/3M1B bioproduction in *Synechocystis*. Interestingly, *pntA* activation led to modest improvements, despite a previous report suggesting its importance primarily under mixotrophic conditions[36]. Similarly, targeting *petH* moderately enhanced compound bioproduction, with sustained effects throughout the experiment. These findings provide the first strategy for NADPH regeneration in the context of producing pyruvate-derived compounds in *Synechocystis*, highlighting that improving NADPH regeneration could be a promising avenue for increasing IB/3M1B production and warrants further investigation. Notably, while our CRISPRa system offers a powerful tool for rapid target testing, the compact genome of *Synechocystis* poses challenges in achieving highly specific activation in some cases as targeting bidirectional promoter regions or operons cannot always be avoided, a challenge previously reported during generation of a CRISPRi library[16]. For example, the *pyk2* promoter region, targeted with the designed gRNAs, overlaps with the promoter region of

slr1362, a gene of unknown function. Thus, we cannot completely exclude that the observed phenotypical changes are only associated with the *pyk2* upregulation and may instead be influenced by the unintended activation of adjacent genes.

We further investigated multiplexing our CRISPRa system for simultaneous targeted gene activation and repression. Our findings confirmed that strong repression could be achieved by targeting within the coding sequence, effectively blocking transcript elongation. Additionally, no dilution effects were observed during multiplexing, enabling strong activation of multiple targets. However, contrary to our GFP activation results, dual gRNAs did not further enhance activation levels of *pyk1* or *pyk2* or improve compound production. This may partly result from reaching an expression threshold for these genes, although additional factors, such as target site accessibility, may also play a role. Interestingly, significant increases in product formation, correlated with elevated transcript level, were achieved when co-targeting *pyk1* and *pyk2* or *pyk2* and *me*, demonstrating a synergetic effect in these strains. While both *acnSP* and *slr6040* repression was strong, only marginal improvements in product formation were observed. A previous study found that a Δ*acnSP* mutant[39] yielded a ~2-fold increase in valine and leucine biosynthesis under higher light conditions (100 µmol photons m^{-2} s^{-1}), while our experiments were performed at 50 µmol photons m^{-2} s^{-1} for consistency with earlier IB/3M1B studies[4,18,29]. This light intensity difference may account for the limited product increase observed in our experiments. Although single *acnSP* targeting had minimal impact, co-targeting *acnSP* with *me* substantially improved IB/3M1B formation. Surprisingly, *me* transcript levels were reduced in the co-targeted strain, potentially due to incompatibility between the co-expressed gRNAs. Interestingly, a 1.5-fold increase of intracellular malate was observed in the Δ*acnSP* mutant[39], which would increase substrate availability for ME. This unexpected behaviour warrants further investigation as unidentified regulatory and metabolic interactions involving AcnSP may influence ME expression or activity. Similarly, strong repression of *slr6040* had limited impact on product formation, despite a previous study reporting a 4.83-fold increase in pyruvate levels in a Δ*slr6040* mutant[41]. Since the exact signal(s) and output of this two-component response regulator are unknown, its lack of effect on product formation remains speculative. Interestingly, co-targeting *slr6040* with activated genes negated the positive impact of gene activation in both multiplexed strains, suggesting that *slr6040* repression leads to system-wide metabolic disturbances. Expanding this multiplexing approach to include targets beyond those directly linked to pyruvate formation would provide valuable insights into regulatory and metabolic processes influencing production. Notably, the results from multiplexed and single-target experiments highlight the need for an improved understanding of system-wide regulatory mechanisms and their impacts in the context of metabolic engineering for compound bioproduction. For instance, shifts in IB/3M1B ratio were observed across several strains when

targeting genes related to pyruvate formation, in accordance with a previously reported phenotype[18]. This warrants extensive omics analysis to uncover associated regulatory mechanisms.

Our CRISPRa system significantly expands the genetic toolbox available for *Synechocystis*, enabling targeted and efficient gene activation for both heterologous and endogenous genes. Our results on IB/3M1B production further highlight its value for rapid target mapping and multiplexed activation for metabolic engineering strategies. Beyond identifying key metabolic reactions influencing compound production, this tool can be employed for promoter optimisation within biosynthetic pathways using randomised gRNAs, a strategy previously demonstrated for violacein biosynthesis[21]. Additionally, CRISPRa-based regulation can be integrated with other regulatory elements to build complex genetic circuits[54,55], allowing cellular signal computing. The potential of this CRISPRa system extends beyond metabolic engineering, offering an interesting opportunity for upregulation of large operons or silent genes[55,56] relevant for fundamental studies. Similarly, genome-wide CRISPRa studies could also be particularly insightful for both applied and fundamental research, enabling the identification of target genes for improved production and characterise gain-of-function phenotypes under various environmental conditions[57], although CRISPRa libraries are still limited in prokaryotes. However, gRNA design remains a critical factor for precise and efficient gene activation. Recent algorithms have refined gRNA prediction[58], although it remains difficult to prevent off-target effects. This challenge will be particularly relevant for CRISPRa libraries in *Synechocystis* as its compact genome contains numerous overlapping promoters, as noted in our study. However, as the CRISPR field advances, new Cas enzymes and engineered variants[26,59] expand targeting capabilities, increasing genome coverage and further broadening applications of CRISPRa systems. Integrating these approaches with our CRISPRa system promises valuable advancements for next-generation metabolic engineering in *Synechocystis*.

Methods

Strains and growth conditions

Escherichia coli DH5α Z1 (Invitrogen) or T7 Express (NEB) were cultivated at 37°C in LB medium supplemented with 50 µg mL^{-1} kanamycin or 50 µg mL^{-1} spectinomycin, when applicable. Background strains of *Synechocystis* sp. PCC 6803 used in this study are listed in Supplementary Table 1. *Synechocystis* strains were routinely grown in BG11 medium[60], supplemented with the appropriate antibiotics (kanamycin: 50 µg mL^{-1} (single antibiotic selection) or 25 µg mL^{-1} (multiple antibiotic selection); spectinomycin: 50 µg mL^{-1} (single antibiotic selection) or 25 µg mL^{-1} (multiple antibiotic selection); chloramphenicol: 25 µg mL^{-1} (single antibiotic selection) or 10 µg mL^{-1} (multiple antibiotic selection); erythromycin: 25 µg

454 mL^{-1}). Cultures were incubated at 30°C, 120 rpm and 50 µmol photons m^{-2} s^{-1}. Seed cultures
455 from cryostocks were inoculated in 6-well plates (Sarstedt) and grown under
456 30 µmol photons m^{-2} s^{-1} illumination. For fluorescence-based tool characterisation, biological
457 replicates were cultivated in 24-well plates (Sarstedt), with 3 glass beads per well to maximise
458 agitation. Tool stability experiments (Supplementary Fig. 1) were conducted in biological
459 triplicates in 100-mL Erlenmeyer flasks containing 25 mL of BG11. For isobutanol and 3-
460 methyl-1-butanol experiments, cultivation conditions are described in the section "Isobutanol
461 and 3-methyl-1-butanol quantification". CRISPRa induction was initiated by the addition of 3
462 mM of L-rhamnose (Sigma-Aldrich) during culture inoculation, unless stated otherwise. Growth
463 profiles were monitored by measuring the optical density at 750 nm using a Hidex Plate
464 Chameleon plate reader. All experimental cultures were inoculated at a starting OD_{750} of 0.1.

465 **Plasmid construction**

466 All plasmids used in this study are listed in Supplementary Table 2. Oligonucleotides were
467 purchased from Integrated DNA Technologies (IDT), with sequences provided in
468 Supplementary Table 3. To construct the initial CRISPRa vector, pBB_CA, a codon-optimised
469 version of *soxS*^{R93A} for *Synechocystis* was synthesised by IDT and inserted into the
470 pBB_dCas12a vector[18] using NEBuilder® HiFi DNA assembly (NEB). For gRNA cloning,
471 complementary 5'-phosphorylated oligonucleotides were purchased (IDT) with the following
472 extensions: AGAT (forward primer) and AGAC (reverse primer), as previously described[61].
473 Primer pairs were annealed in nuclease-free Duplex buffer (IDT) by combining 2 µL of each
474 primer (100 µM) with 46 µL Duplex buffer and incubating the reaction for 2 min at 94°C followed
475 by gradual cooling to room temperature. The resulting annealed gRNAs were cloned into AarI-
476 digested pBB_CA. pBB_CA and its gRNA-containing derivatives featured the broad-host-
477 range RSF1010 replicon and mobilisation region[62]. For genomic integration of GFP into the
478 NS1 (*slr0168*) site[63], the GFP coding sequence was amplified from pEB1-wtGFP[64] (purchased
479 from Addgene; accession number #103978) using Phusion™ Hot Start II DNA Polymerase
480 (ThermoFisher) and subsequently fused to the respective promoters via overlapping PCR. The
481 resulting constructs were cloned into the P3 vector[4] using EcoRI and NotI restriction enzymes
482 (ThermoFisher Scientific). All plasmids were confirmed by Sanger sequencing (Eurofins).

483 ***Synechocystis* natural transformation and conjugation**

484 Integrative plasmids were transformed into *Synechocystis* via natural transformation as
485 previously described[29]. Briefly, cultures were grown to an OD_{750} of ~1.0, centrifuged at 6 000
486 x *g* for 10 min, washed twice in BG11 medium and resuspended at a final cell density of 1 x
487 10^9 cells mL^{-1}. 400 µL of cell suspension were incubated with 4 µg of plasmid DNA for 4-5
488 hours at 30°C, 120 rpm and 50 µmol photons m^{-2} s^{-1} and plated on nitrocellulose membranes

placed on non-selective BG11 agar plates. After 20-24 hours, the membranes were transferred to selective plates with the appropriate antibiotic(s) and incubated at 30°C and 50 µmol photons m^{-2} s^{-1} until colonies appeared (7-10 days). Colonies were restreaked onto selective BG11 agar plates and screened for positive genomic integration by PCR with DreamTaq DNA polymerase (ThermoFisher). Selected colonies were inoculated in selective BG11 medium in 6-well plates and propagated until fully segregated.

For self-replicating plasmids, a triparental conjugation method was used, as previously described[29]. Briefly, the cargo *E. coli* strain carrying the target plasmid and the helper strain[65] HB101 containing the pRL443-Amp^R plasmid were grown overnight at 37°C in LB, supplemented with 50 µg mL^{-1} kanamycin and 100 µg mL^{-1} ampicillin, respectively. After overnight growth, 1 mL of each *E. coli* strain and the recipient *Synechocystis* strain (at OD_{750} = ~1.0) was centrifuged at 3 000 x *g* for 5 min and resuspended in fresh LB or BG11. 500 µL of cell suspension of cargo strain and helper strain were combined and washed twice in LB. Concurrently, *Synechocystis* cells were washed twice in BG11. 50 µL of *Synechocystis* cell suspension were added to the *E. coli* mixture, incubated for 1.5-2 hours at 30°C, 120 rpm and 50 µmol photons m^{-2} s^{-1} and plated on nitrocellulose membranes on non-selective BG11 plates. After 20-24 hours, the membranes were transferred to selective BG11 plates and incubated at 30°C and 50 µmol photons m^{-2} s^{-1} until colonies formed (5-7 days). Single colonies were restreaked onto selective BG11 plates and analysed by colony PCR. Positive transformants were inoculated in 6-well plates in selective BG11 and used for subsequent experiments.

Fluorescence measurements

GFP fluorescence was quantified with a Hidex Plate Chameleon plate reader with an excitation at 390 nm and emission at 500 nm. Optical density was simultaneously measured at 750 nm. Fluorescence measurements were normalised to OD_{750}.

RNA extraction and RT-qPCR

For RNA extraction, cells were harvested at 3 000 x *g* for 10 min and washed twice with sterile H_2O. Cells pellets were stored at -80°C until further processing. Pellets were thawed and resuspended in 500 µL Trizol (Sigma-Aldrich). 0.2 g of acid-washed glass beads (Sigma-Aldrich) were added to cell suspensions to facilitate cell disruption. Cell lysis was carried out using a Precellys-24 bead beater (Bertin Instruments) with 3 consecutive cycles of 30 sec at 3 000 x *g* followed by 2 min on ice between cycles. To remove cell debris and glass beads after lysis, samples were centrifuged at 12 000 x *g* at 4°C for 10 min and supernatants were collected. RNA was isolated using the Direct-zol™ RNA Microprep kit (Zymo Research) following the manufacturer's protocol, excluding the DNase treatment step. RNA

concentrations were determined using a Nanodrop™ 2000 spectrophotometer (Thermo Scientific) and 1 µg of RNA was treated with DNase I (ThermoFisher) in two consecutive reactions to eliminate potential genomic DNA. The resulting samples were then purified a second time with the Direct-zol™ RNA Microprep kit to increase sample purity. For cDNA synthesis, 150 ng of RNA was used as template for the iScript™ cDNA synthesis kit (BIO-RAD) according to the manufacturer's recommendations. Real-time quantitative PCR (RT-qPCR) was performed on 5 ng of cDNA with iTaq Universal SYBR Green Supermix (BIO-RAD) in a CFX Connect Real Time PCR system (BIO-RAD). The *rnpB* gene, encoding the RNA subunit of ribonuclease P, served as the reference gene, with primers previously described[66]. Other primers sequences are provided in Supplementary Table 3. Each sample was analysed in three technical replicates, and relative gene expression levels were calculated using the $2^{-\Delta\Delta CT}$ method[67].

Isobutanol and 3-methyl-1-butanol quantification

For production experiments, seed cultures were inoculated in 6-well plates in selective BG11 supplemented with appropriate antibiotics and incubated at 30°C and 30 µmol photons m^{-2} s^{-1}. 25 mL of BG11 supplemented with 50 mM $NaHCO_3$ (Sigma-Aldrich), and 3 mM L-rhamnose were inoculated at OD_{750} = 0.1 from seed cultures in BioLite 25 cm^2 plug-sealed tissue culture flasks (ThermoFisher Scientific), as previously described[29]. The cultures were horizontally shaken at 120 rpm under 50 µmol photons m^{-2} s^{-1} illumination at 30°C. Every second day, 2 mL of cultures were replaced by 2 mL of BG11 supplemented with 500 mM $NaHCO_3$, 3 mM L-rhamnose and appropriate antibiotics. OD_{750} was monitored daily through measurement with a Hidex Plate Chameleon plate reader and product formation was quantified on days 3, 4, 6, 8 and 10 for experiments with multiple *kivD*^{S286T} copies or on days 2, 3 and 4 for target mapping. Cultures were performed in biological triplicates.

Isobutanol and 3-methyl-1-butanol were extracted from culture samples using a dichloromethane (DCM) extraction method previously described[29]. Both products were quantified by gas chromatography using a PerkinElmer GC 580 system equipped with a flame ionization detector (FID) and an Elite-WAX Polyethylene Glycol Series Capillary column (30 m × 0.25 mm × 0.25 µm, PerkinElmer) with nitrogen as the carrier gas at a rate of 10 mL min^{-1}. The injector and detector temperatures were set at 220 °C and 240 °C, respectively. The GC results obtained were analyzed using TotalChrom Navigator version 6.3.2.

Statistical analysis

All data are presented as the mean value ± standard deviation (SD). Experiments for fluorescence-based tool characterisation had a sampling size of n ≥ 5. All IB/3M1B experiments were performed in biological triplicates (n=3). Statistical significance was

determined using an unpaired two-tailed *t*-test. Relevant p-values are reported on the respective figures (ns (not significant) > 0.05; * < 0.05; ** < 0.01; *** < 0.001.).

Data availability

The main data supporting the findings of this study are available in the paper, supplementary material and source data.

References

1. Kukil, K. & Lindberg, P. Metabolic engineering of *Synechocystis* sp. PCC 6803 for the improved production of phenylpropanoids. *Microb. Cell Fact.* **23**, 1–14 (2024).
2. Zhong, J. *et al.* Engineering cyanobacteria as a new platform for producing taxol precursors directly from carbon dioxide. *Biotechnol. Biofuels Bioprod.* **17**, 1–15 (2024).
3. Yoo, D. *et al.* Metabolic Engineering for redirecting carbon to enhance the fatty acid content of *Synechocystis* sp. PCC6803. *Biotechnol. Bioprocess Eng.* **28**, 274–280 (2023).
4. Xie, H., Kjellström, J. & Lindblad, P. Sustainable production of photosynthetic isobutanol and 3-methyl-1-butanol in the cyanobacterium *Synechocystis* sp. PCC 6803. *Biotechnol. Biofuels Bioprod.* **16**, 1–17 (2023).
5. Germann, A. T. *et al.* A systematic overexpression approach reveals native targets to increase squalene production in *Synechocystis* sp. PCC 6803. *Front. Plant Sci.* **14**, 1–12 (2023).
6. Rodrigues, J. S., Bourgade, B., Galle, K. R. & Lindberg, P. Mapping competitive pathways to terpenoid biosynthesis in *Synechocystis* sp . PCC 6803 using an antisense RNA synthetic tool. *Microb. Cell Fact.* 1–16 (2023).
7. Mustila, H., Kugler, A. & Stensjö, K. Isobutene production in *Synechocystis* sp. PCC 6803 by introducing α-ketoisocaproate dioxygenase from *Rattus norvegicus*. *Metab. Eng. Commun.* **12**, (2021).
8. Pacesa, M., Pelea, O. & Jinek, M. Past, present, and future of CRISPR genome editing technologies. *Cell* **187**, 1076–1100 (2024).
9. Zhang, R., Xu, W., Shao, S. & Wang, Q. Gene silencing through CRISPR interference in bacteria: current advances and future prospects. *Front. Microbiol.* **12**, 1–8 (2021).
10. Bikard, D. *et al.* Programmable repression and activation of bacterial gene expression using an engineered CRISPR-Cas system. *Nucleic Acids Res.* **41**, 7429–7437 (2013).
11. Dong, C., Fontana, J., Patel, A., Carothers, J. M. & Zalatan, J. G. Synthetic CRISPR-Cas gene activators for transcriptional reprogramming in bacteria. *Nat. Commun.* **9**, (2018).
12. Villegas Kcam, M. C., Tsong, A. J. & Chappell, J. Rational engineering of a modular bacterial CRISPR-Cas activation platform with expanded target range. *Nucleic Acids Res.* **49**, 4793–4802 (2021).
13. Schilling, C., Koffas, M. A. G., Sieber, V. & Schmid, J. Novel prokaryotic CRISPR-Cas12a-based tool for programmable transcriptional activation and repression. *ACS Synth. Biol.* **9**, 3353–3363 (2021).

14. Bernardi, A. & Spahr, P. F. Nucleotide sequence at the binding site for coat protein on RNA of bacteriophage R17. *Proc. Natl. Acad. Sci. U. S. A.* **69**, 3033–3037 (1972).

15. Miao, R., Jahn, M., Shabestary, K., Peltier, G. & Hudson, E. P. CRISPR interference screens reveal growth–robustness tradeoffs in *Synechocystis* sp. PCC 6803 across growth conditions. *Plant Cell* **35**, 3937–3956 (2023).

16. Yao, L. *et al.* Pooled CRISPRi screening of the cyanobacterium *Synechocystis* sp PCC 6803 for enhanced industrial phenotypes. *Nat. Commun.* **11**, (2020).

17. Liu, D., Johnson, V. M. & Pakrasi, H. B. A reversibly induced CRISPRi system targeting Photosystem II in the cyanobacterium *Synechocystis* sp. PCC 6803. *ACS Synth. Biol.* **9**, 1441–1449 (2020).

18. Xie, H., Bourgade, B., Stensjö, K. & Lindblad, P. dCas12a-mediated CRISPR interference for multiplex gene repression in cyanobacteria for enhanced isobutanol and 3-methyl-1-butanol production. *Bioresour. Technol.* Under revision.

19. Fontana, J. *et al.* Effective CRISPRa-mediated control of gene expression in bacteria must overcome strict target site requirements. *Nat. Commun.* **11**, 1–11 (2020).

20. Behle, A., Saake, P., Germann, A. T., Dienst, D. & Axmann, I. M. Comparative dose-response analysis of inducible promoters in cyanobacteria. *ACS Synth. Biol.* **9**, 843–855 (2020).

21. Liu, Y., Wan, X. & Wang, B. Engineered CRISPRa enables programmable eukaryote-like gene activation in bacteria. *Nat. Commun.* **10**, (2019).

22. Fontana, J., Sparkman-Yager, D., Zalatan, J. G. & Carothers, J. M. Challenges and opportunities with CRISPR activation in bacteria for data-driven metabolic engineering. *Curr. Opin. Biotechnol.* **64**, 190–198 (2020).

23. Kiattisewee, C. *et al.* Portable bacterial CRISPR transcriptional activation enables metabolic engineering in *Pseudomonas putida*. *Metab. Eng.* **66**, 283–295 (2021).

24. Ameruoso, A., Kcam, M. C. V., Cohen, K. P. & Chappell, J. Activating natural product synthesis using CRISPR interference and activation systems in *Streptomyces*. *Nucleic Acids Res.* **50**, 7751–7760 (2022).

25. Englund, E., Shabestary, K., Hudson, E. P. & Lindberg, P. Systematic overexpression study to find target enzymes enhancing production of terpenes in *Synechocystis* PCC 6803, using isoprene as a model compound. *Metab. Eng.* **49**, 164–177 (2018).

26. Guo, L. Y. *et al.* Multiplexed genome regulation in vivo with hyper-efficient Cas12a. *Nat. Cell Biol.* **24**, 590–600 (2022).

27. Vasudevan, R. *et al.* Cyanogate: A modular cloning suite for engineering cyanobacteria based on the plant moclo syntax. *Plant Physiol.* **180**, 39–55 (2019).

28. Miao, R., Xie, H. & Lindblad, P. Enhancement of photosynthetic isobutanol production in engineered cells of *Synechocystis* PCC 6803. *Biotechnol. Biofuels* **11**, 1–9 (2018).

29. Xie, H. & Lindblad, P. Expressing 2-keto acid pathway enzymes significantly increases photosynthetic isobutanol production. *Microb. Cell Fact.* **21**, 1–17 (2022).

30. Karikomi, M., Katayama, N. & Osanai, T. Pyruvate kinase 2 from *Synechocystis* sp. PCC 6803 increased substrate affinity via glucose-6-phosphate and ribose-5-phosphate for phosphoenolpyruvate consumption. *Plant Mol. Biol.* **114**, 1–12 (2024).

31. Katayama, N., Iwazumi, K., Suzuki, H., Osanai, H. & Ito, S. Malic enzyme, not malate dehydrogenase, mainly oxidizes malate that originates from the tricarboxylic acid cycle

in cyanobacteria. *mBio*. **13** (2022).

32. Hidese, R., Matsuda, M., Osanai, T., Hasunuma, T. & Kondo, A. Malic enzyme facilitates D-lactate production through increased pyruvate supply during anoxic dark fermentation in *Synechocystis* sp. PCC 6803. *ACS Synth. Biol.* **9**, 260–268 (2020).

33. Liu, W., Zhang, R., Wei, M., Cao, Y. & Xian, M. Increasing the pyruvate pool by overexpressing phosphoenolpyruvate carboxykinase or triosephosphate isomerase enhances phloroglucinol production in *Escherichia coli*. *Biotechnol. Lett.* **42**, 633–640 (2020).

34. Rieble, S. & Beale, S. I. Structure and expression of a cyanobacterial *ilvC* gene encoding acetohydroxyacid isomeroreductase. *J. Bacteriol.* **174**, 7910–7918 (1992).

35. Hao, Y. *et al.* High-yield production of L-valine in engineered *Escherichia coli* by a novel two-stage fermentation. *Metab. Eng.* **62**, 198–206 (2020).

36. Kämäräinen, J. *et al.* Pyridine nucleotide transhydrogenase PntAB is essential for optimal growth and photosynthetic integrity under low-light mixotrophic conditions in *Synechocystis* sp. PCC 6803. *New Phytol.* **214**, 194–204 (2017).

37. Grzyb, J., Gieczewska, K., Łabuz, J. & Sztatelman, O. Detailed characterization of *Synechocystis* PCC 6803 ferredoxin:NADP+ oxidoreductase interaction with model membranes. *Biochim. Biophys. Acta - Biomembr.* **1860**, 281–291 (2018).

38. Luo, W. *et al.* Strengthening NADPH regeneration for improving photo-biocatalytic ketones asymmetric reduction reaction by *Synechocystis* through overexpression of FNR. *Catal. Letters* **148**, 1714–1722 (2018).

39. de Alvarenga, L. V., Hess, W. R. & Hagemann, M. AcnSP – A novel small protein regulator of aconitase activity in the cyanobacterium *Synechocystis* sp. PCC 6803. *Front. Microbiol.* **11**, 1–12 (2020).

40. Carrieri, D. *et al.* Transcriptome and proteome analysis of nitrogen starvation responses in *Synechocystis* 6803 ΔglgC, a mutant incapable of glycogen storage. *Algal Res.* **21**, 64–75 (2017).

41. Shi, M., Chen, L. & Zhang, W. Regulatory diversity and functional analysis of two-component systems in cyanobacterium *Synechocystis* sp. PCC 6803 by GC-MS based metabolomics. *Front. Microbiol.* **11**, 1–16 (2020).

42. Matthias, K. *et al.* Comparative analysis of the primary transcriptome of *Synechocystis* sp. PCC 6803. *DNA Res.* **21**, 527–539 (2014).

43. Suzuki, I., Simon, W. J. & Slabas, A. R. The heat shock response of *Synechocystis* sp. PCC 6803 analysed by transcriptomics and proteomics. *J. Exp. Bot.* **57**, 1573–1578 (2006).

44. Kobayashi, K., Yoneda, K., Maeda, Y. & Suzuki, I. Transcriptomic analysis reveals insights into the responses of *Synechocystis* sp. PCC 6803 to acidification during cultivation with ammonium salts as a nitrogen source. *J. Biosci. Bioeng.* **138**, 261–270 (2024).

45. Bolay, P. *et al.* The transcriptional regulator RbcR controls ribulose-1,5-bisphosphate carboxylase/oxygenase (RuBisCO) genes in the cyanobacterium *Synechocystis* sp. PCC 6803. *New Phytol.* **235**, 432–445 (2022).

46. Gao, H. *et al.* Engineering of microbial cells for L-valine production: challenges and opportunities. *Microb. Cell Fact.* **20**, 1–16 (2021).

47. Jones, P. R. Genetic instability in cyanobacteria - An elephant in the room? *Front.*

Bioeng. Biotechnol. **2**, 1–5 (2014).

48. Sun, H. *et al.* Engineered hypermutation adapts cyanobacterial photosynthesis to combined high light and high temperature stress. *Nat. Commun.* **14**, 1–20 (2023).

49. Guillaume, M. C. & Branco dos Santos, F. Assessing and reducing phenotypic instability in cyanobacteria. *Curr. Opin. Biotechnol.* **80**, 102899 (2023).

50. Haghighi, O. In Silico study of the structure and ligand preference of pyruvate kinases from cyanobacterium *Synechocystis* sp. PCC 6803. *Appl. Biochem. Biotechnol.* **193**, 3651–3671 (2021).

51. Kaniya, Y. *et al.* Deletion of the transcriptional regulator cyAbrB2 deregulates primary carbon metabolism in *Synechocystis* sp. PCC 6803. *Plant Physiol.* **162**, 1153–1163 (2013).

52. Young, J. D., Shastri, A. A., Stephanopoulos, G. & Morgan, J. A. Mapping photoautotrophic metabolism with isotopically nonstationary 13C flux analysis. *Metab. Eng.* **13**, 656–665 (2011).

53. Yoshikawa, K., Hirasawa, T. & Shimizu, H. Effect of malic enzyme on ethanol production by *Synechocystis* sp. PCC 6803. *J. Biosci. Bioeng.* **119**, 82–84 (2015).

54. Bhokisham, N. *et al.* A redox-based electrogenetic CRISPR system to connect with and control biological information networks. *Nat. Commun.* **11**, (2020).

55. Call, S. N. & Andrews, L. B. CRISPR-Based approaches for gene regulation in non-model bacteria. *Front. Genome Ed.* **4**, 1–17 (2022).

56. Ke, J. *et al.* CRAGE-CRISPR facilitates rapid activation of secondary metabolite biosynthetic gene clusters in bacteria. *Cell Chem. Biol.* **29**, 696-710.e4 (2022).

57. Sanson, K. R. *et al.* Optimized libraries for CRISPR-Cas9 genetic screens with multiple modalities. *Nat. Commun.* **9**, 1–15 (2018).

58. Wright, G., Emrich, S. J., Rodriguez, A. & Clark, P. L. CHARMING : Harmonizing synonymous codon usage to replicate a desired codon usage pattern. 221–231 (2022). doi:10.1002/pro.4223

59. Xu, X. *et al.* Engineered miniature CRISPR-Cas system for mammalian genome regulation and editing. *Mol. Cell* **81**, 4333-4345.e4 (2021).

60. Rippka, R., Deruelles, J. & Waterbury, J. B. Generic assignments, strain histories and properties of pure cultures of cyanobacteria. *J. Gen. Microbiol.* **111**, 1–61 (1979).

61. Ungerer, J. & Pakrasi, H. B. Cpf1 is a versatile tool for CRISPR genome editing across diverse species of cyanobacteria. *Sci. Rep.* **6**, 1–9 (2016).

62. Taton, A. *et al.* Broad-host-range vector system for synthetic biology and biotechnology in cyanobacteria. *Nucleic Acids Res.* **42**, 1–16 (2014).

63. Williams, J. G. K. Construction of specific mutations in Photosystem II photosynthetic reaction center by genetic engineering methods in *Synechocystis* 6803. *Methods Enzymol.* **167**, 766–778 (1988).

64. Balleza, E., Kim, J. M. & Cluzel, P. Systematic characterization of maturation time of fluorescent proteins in living cells. *Nat. Methods.* **15**, 47–51 (2018).

65. Elhai, J., Vepritskiy, A., Muro-Pastor, A. M., Flores, E. & Wolk, C. P. Reduction of conjugal transfer efficiency by three restriction activities of *Anabaena* sp. strain PCC 7120. *J. Bacteriol.* **179**, 1998–2005 (1997).

66. Pinto, F., Pacheco, C. C., Ferreira, D., Moradas-Ferreira, P. & Tamagnini, P. Selection of suitable reference genes for RT-qPCR analyses in cyanobacteria. *PLoS One* **7**, 1–9 (2012).

67. Livak, K. J. & Schmittgen, T. D. Analysis of relative gene expression data using real-time quantitative PCR and the 2-ΔΔCT method. *Methods* **25**, 402–408 (2001).

Acknowledgments

We acknowledge financial support from Formas - A Swedish Research Council for Sustainable Development (project no. 2021-01669).

Author contributions

BB: Conceptualisation; Data curation; Formal analysis; Investigation; Methodology; Validation; Visualization; Writing - original draft; Writing - review & editing. **HX**: Development of background strains ddh_kivD, HX11 and HX51; Technical support for IB/3M1B quantification; Writing - review & editing. **PL**: Writing - review & editing. **KS**: Funding acquisition; Project administration; Resources; Supervision; Writing - review & editing. All authors read and approved the final draft of the manuscript.

Competing interests

The authors declare no competing interests.